Chemical Communications

COMMUNICATION

Spontaneous reaction between uncharged lithium iron silicate cathode and $LiPF_6$-based electrolyte

Received 00th January 20xx,
Accepted 00th January 20xx

DOI: 10.1039/x0xx00000x

www.rsc.org/

Zachary Arthur[1], Hsien-Chieh Chiu[2], Xia Lu[2], Ning Chen[3], Vincent Emond[1], Karim Zaghib[4], De-Tong Jiang [1,*], and George P. Demopoulos [2,*]

The reaction between uncharged Li_2FeSiO_4 (LFS) cathode and $LiPF_6$-EC/DMC electrolyte is revealed by *in situ* XANES in coin cells. The study shows clear evidence of delithiation and iron oxidation in LFS prior to cycling. Subsequent cycling appears to partially restore the original lithiation level, an observation that needs to be taken into consideration in future LFS development work.

Today, Lithium-ion batteries (LIBs) are ubiquitous, they can be found everywhere from our portable electronics, to the automotive and renewable energy sector [1, 2]. Indeed, LIBs have been a crucial enabling component in the development of many of the transformative technologies we have seen emerging since the early 2000s, e.g. smart phones, electric cars, etc. In order to improve upon the current generation of LIBs it is necessary to develop low cost, safe, and high energy density cathode materials. One material class that has been garnering great interest in this respect is that of Li_2MSiO_4 (LMS, M = Fe, Mn) silicates, an olivine structure that has a theoretical charge capacity of 330 mAh / g [3, 4], double of that of lithium iron phosphate[5].

The challenges currently facing the development of LFS (M=Fe) cathodes are not trivial. The charge compensation mechanism for $Li_{1-x}FeSiO_4$, 0<x<1, is still not fully understood[6, 7], and the extraction of more than one lithium results in capacity loss, attributed to Fe-Li anti-site defects and phase transitions induced during charging-discharging[6, 8]. Meanwhile, the compatibility between electrolyte and the cathode may be cause of concern as well[9, 10], especially in this case because the fluorine in the typical, most popular $LiPF_6$-based electrolyte, could react with the Si species in LFS[11-13]. However, the preceding studies have either looked into the LFS-electrolyte interaction issue by post mortem (i.e. after cycling) *ex situ* surface characterization with techniques like XPS[12] or by bulk characterization using XRD and EDX following aggressive ageing at 60°C[11]. Understanding electrode-electrolyte interphasial phenomena as proven in the case of the well-known solid-electrolyte interphase (SEI)[9, 14] is crucial for the development of robust silicate cathode Li-ion batteries. In particular *in situ* probing of these phenomena can provide critical missing links in this regard.

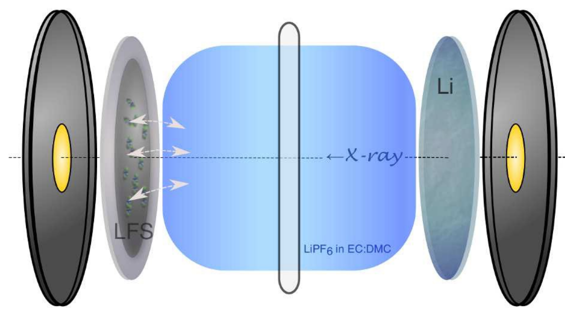

Fig. 1 Schematic of the *in situ* CR2032 coin cell with Kapton® windows used for XANES monitoring of the LFS-Electrolyte interaction (depicted with arrows at the solid-electrolyte interphase).

In this study, the spontaneous reaction between uncharged (prior to cycling) Li_2FeSiO_4 (LFS) cathode and $LiPF_6$-EC/DMC electrolyte is studied by *in situ* X-ray absorption near-edge spectroscopy (XANES) using coin cells. The LFS cathode (80% LFS, 10% acetylene black and 10% PVDF) featured Li_2FeSiO_4 nanoparticles prepared via an organic-assisted hydrothermal-annealing (180°C and 400°C, respectively) synthesis method[15]. The cathode slurry was rolled onto an Al foil current collector, and assembled into a modified CR2032 coin cell with a Li anode, a 25 µm PP/PE/PP separator (Celgard 2325), and using 1M of $LiPF_6$ in EC/DMC (1:1 by volume) as the electrolyte. A schematic view of this setup can be seen in Figure 1.

The pristine LFS sample was characterized with SEM, XANES, and synchrotron radiation XRD. From SEM imaging and processing using Image J [16] (Figure 2a), the particle area was determined to be on average 1270 ± 285 nm^2. This reveals that the pristine material composed of nanoparticles on the order of ~40 nm and is in the form of aggregates[15]. Synchrotron-radiation XRD and XANES measurements were taken at the HXMA beamline at the Canadian

[a] Department of Physics, University of Guelph, 50 Stone Road East, Guelph, ON N1G 2W1, Canada.
[b] Materials Engineering, McGill University, Montreal, QC H3A 0C5, Canada.
[c] Canadian Light Source, 44 Innovation Boulevard, Saskatoon, SK S7N 2V3, Canada.
[d] Institut de recherche d'Hydro-Québec (IREQ), Varennes, QC J3X 1S1, Canada.
*Corresponding authors: djiang@uoguelph.ca and george.demopoulos@mcgill.ca

Light Source (CLS)[17]. The CLS HXMA wiggler was running at 1.9 T and the CLS storage ring was with a 250 mA current. The Si(111) monochromator crystals in combination with Rh coated pre-mono collimating mirror and post-mono toroidal focusing mirror were used. For the XANES measurements, both the incoming and transmitted X-ray intensity were monitored by ionization chambers filled with He gas, and the fluorescence yield was monitored by a Lytle detector filled with N_2 gas, data was reduced using Athena[18];

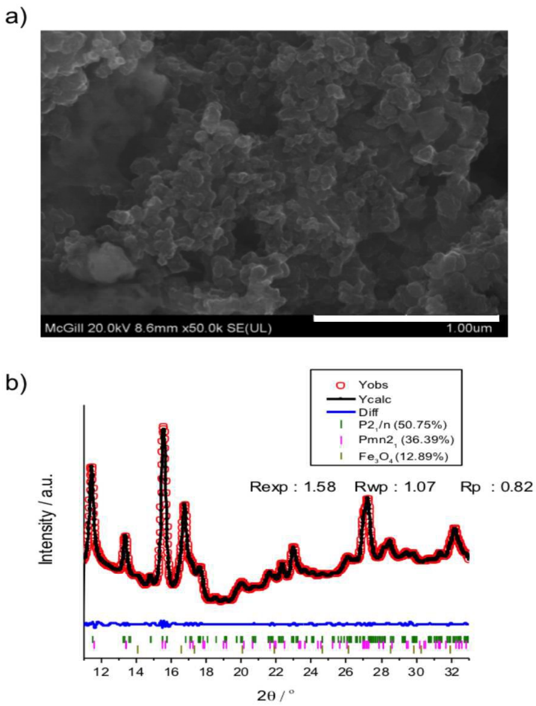

Fig. 2 Morphology and phase identification of the pristine LFS sample as characterized by SEM and SR-XRD, a) SEM image taken at 20.0kV, shows the aggregation of the LFS nanoparticles, b) Reitveld refinement of the SR-XRD data, revealing an approximate phase mixture 3:2 of monoclinic and orthorhombic structures, respectively.

for XRD detection a mar345 image plate was used to record the Debye-Scherrer rings from a modified CR2032 cell (Figure 1), rings were integrated using fit2D[19]. XANES were measured at the Fe K-edge and the XRD patterns were recorded at 17 keV photon energy; energy calibration was performed by determining the first inflection point of standard Fe and Yt XANES, for the respective energies. The mar345 detector distance was calibrated using a NIST LaB_6 powder mounted inside of an *in situ* cell case, and fit2D's calibration function. The as-prepared material was found to be a mixture of approximately 3:2 of monoclinic $P2_1/n$ (γ_s) and the "low temperature" orthorhombic $Pmn2_1$ (β_{II}) phases (Figure 2b), respectively[20].

In situ XANES measurements of the cathode were performed on the initial uncharged battery state (96 hours following the coin cell assembly during which LFS was in contact with 1M of $LiPF_6$ in EC/DMC solvent) as well as after cycling the cell at C/20 rate for a single Li extraction-insertion (formation) cycle. The "uncharged" cell is labelled, $20C_0$ and the "cycled" cell, $20D_f$.

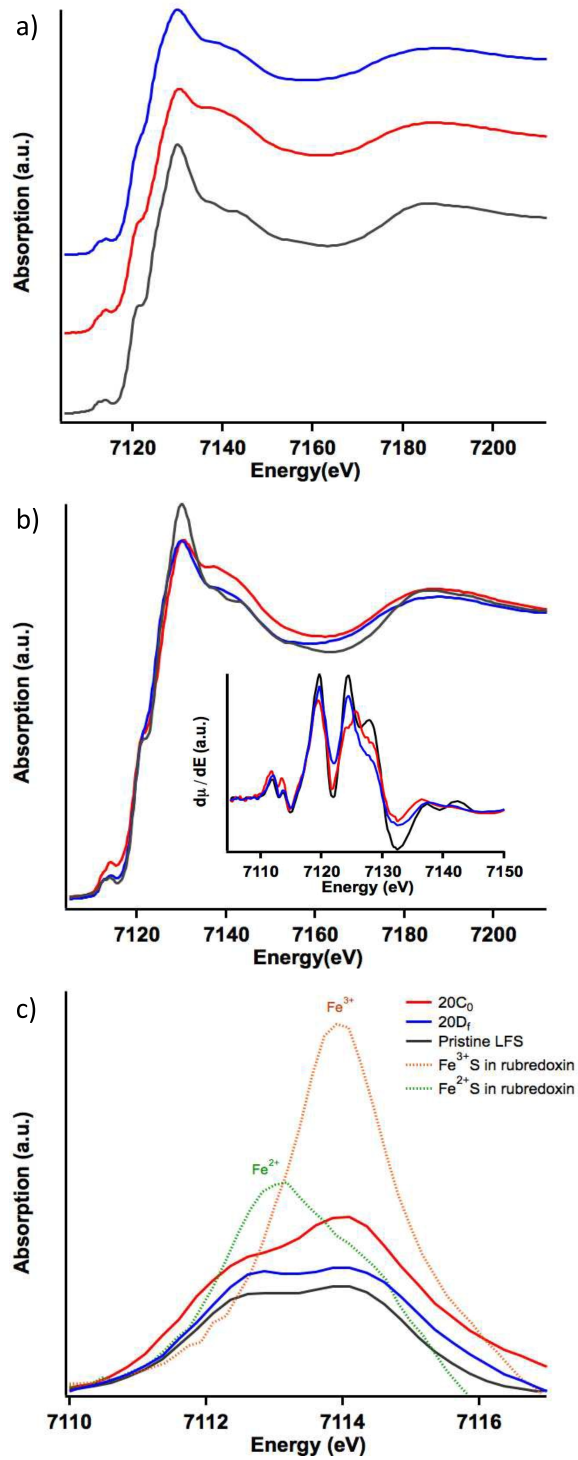

Fig. 3 XANES measurements of LFS in different charging states: a) (black) pristine LFS, (red) $20C_0$ cathode inside the uncharged coin cell (LFS in contact with $LiPF_6$ EC/DEC electrolyte), (blue) $20D_f$ cathode after cycling at 1/20 C; b) components from (a) overlaid for direct comparison, inset: derivative spectra highlighting the pre-edge – white-line region; c) zoomed-in pre-edge region with background subtracted, also included are the reference spectra pre-edges of FeS_4 in rubredoxin reduced and oxidized states, respectively.

These three samples correspond to the same electrochemical state, and represent the typical spectra we have measured for this material in these electrochemical states.

The normalized Fe K-edge XANES spectra in Fig. 3a show the results for the different LFS samples. The differences among the electronic structures of the three LFS samples are subtle but nevertheless noticeable. The first of which is that, the pristine sample (Figure 3a,b black) shows well-resolved spectral features following the "white-line" area (i.e. the strongest peak area above the edge jump), compared to the other two samples: $20C_0$ and $20D_f$, uncharged and cycled (formation cycle), respectively. This reflects the increase of structural disorder in samples $20C_0$ and $20D_F$‡. For sample $20C_0$ this means that the contact of LFS cathode with the electrolyte inside the coin cell (96 hours storage time at room temperature) has triggered a spontaneous reaction resulting in noticeable structural change in the cathode material. Upon cycling (formation cycle) however, the cathode ($20D_f$ sample) is seen to restore, in part, its local structure towards that of the pristine sample. This can be seen by comparing the post-"white-line" region (Fig. 3b) and more clearly in the derivative spectra. The first derivatives of the XANES spectra for the three samples are shown in Figure 3b inset, and were calculated using the central difference method. Here the restoration trend can be seen following the peak around 7125 eV. This corresponds to the inflection point just before the "white-line" region (where the spectra are free of any pre-edge effects caused by Jahn-Teller distortions). Specifically this derivative peak moves toward higher energy in the uncharged material and then returns to the same position as the pristine upon cycling.

The previous observations are echoed by the trend of the pre-edge features (Figure 3c), that is the pristine sample has the lowest overall pre-edge intensity while the uncharged has the highest. This feature is reflective of the distortion of the FeO_4 tetrahedron via Jahn-Teller effect[21]. Here the cycled cathode pre-edge intensity is between that of the other two, indicating again a certain level of structural restoration. In addition to the overall pre-edge intensity differences, Fig. 3c shows clearly the varied intensity distribution profiles among the three, which are related to the underlying spectral components of different oxidation species[22]. To facilitate further analysis, in Figure 3c two low-temperature reference phases have been included for the ferrous and ferric states of Fe. These are the tetrahedrally coordinated $Fe^{2+}S_4$ and $Fe^{3+}S_4$ found in rubredoxin[23]. The ratio of the pre-edge features contributed by the ferrous and ferric states were fit using a linear combination[18] of pre-edges from the $Fe^{2+}S_4$ and $Fe^{3+}S_4$ reference data. The fitting results are summarized in Figure 4, each fit performed reported an R-factor[18] less than 0.025. The results show that the Fe site within the LFS matrix indeed became oxidized (likely with the reduction of the electrolyte) during the 96 hour interphasial interaction; upon cycling, this state was partially restored towards the original ferrous/ferric ratio in the pristine sample.

The relative spectral intensity increase of Fe^{3+} in the uncharged cathode compared to the pristine (Fig. 4) is usually a direct fingerprint of the charge compensation process throughout a normal charging sequence. Here however, no external charging has been applied. In this case, in the absence of any applied current, this pre-edge profile variance indicates delithiation of the material as a consequence of reduction of an electrolytic component. Previous research by Dippel et al.[13] involving the ageing of the LFS material in hot (60°C) $LiPF_6$-EC/DMC organic electrolyte concluded that LFS converts under those conditions to Li_2SiF_6 with simultaneous dissolution of iron into the electrolyte. No delithiation or iron oxidation was reported as observed here. The same group in a follow up study[11] commented that the electrolyte thermally decomposed at 60°C even in the absence of LFS hence the previous high temperature study appears to have observed reactions not necessarily operational in an actual coin cell that is typically used at lower temperatures. As per other electrode-electrolyte interphase systems[14] it is likely that reduction of the organic carbonate solvent molecules takes place on the surface of LFS leading to iron oxidation.

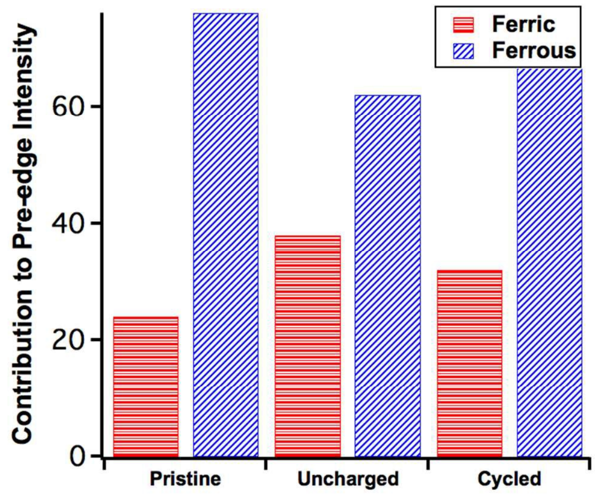

Fig. 4 Category plot of the Fe^{2+} and Fe^{3+} contribution to the pre-edge for the pristine material, uncharged ($20C_0$) and cycled ($20D_f$), as determined by a linear combination fit with FeS_4 reference compounds: low-temperature XAS from molecular FeS_4 in rubredoxin

As a plausible mechanism for the observed spontaneous reaction between the $LiPF_6$-EC/DMC electrolyte and Li_2FeSiO_4 (LFS) we propose tentatively the following sequence. Fluoride anions (released from $LiPF_6$) owing to their well-known propensity to form Si-F groups (such as SiF^{6-}), are envisaged to react with the surface of LFS as noted in Ensling et al.'s XPS analysis[12]. Such Si-F interaction on the LFS surface would weaken the Fe^{II}-SiO_4 bonding rendering iron (II) prone to oxidation via reduction of electrolyte components such as EC and DMC that is well established in literature[13]. In other words the oxidation of Fe(II) in this case is rendered feasible because of the F-induced weakening of the Fe^{II}-Si-O_x bonding caused by the Si-F interaction. Further detailed investigations would be needed to allow for deeper understanding of this reaction and we are in the process of doing that.

Beyond the observation of the spontaneous reaction (while the cell is uncharged) another important revelation of this work is the finding that after the first charge-discharge cycle there is (at least in part) restoration of the LFS structure as evident by the oxidation state of iron. Thus the relative spectral intensity of Fe^{3+} was reduced from ~ 37% at the "uncharged" state (i.e. following the spontaneous reaction) to approximately 32% at the discharged state (after the formation cycle) compared to 24% for the particular pristine sample used in this work (Fig. 4). It should be pointed out that the cycling process is known to produce a crystalline phase change in the pristine material [8, 15], which could affect the overall intensity of the pre-edge features. The above analysis is concerned only with the relative ratio of Fe^{2+} and Fe^{3+} contributions to the overall pre-edge spectrum. What these results imply in terms of battery performance, however, is that though the reduction of electrolyte does occur spontaneously and slightly increases the state-of-charge (SOC) of LFS during coin cell pre-cycling storage, that the accompanying delithiation reaction is at least in part reversible. Given these findings further research is warranted not only in elucidating this complex interphasial reaction but also in assessing its role in the overall structural stability and loss of irreversibility during cycling of this important cathode material. Study of alternative to F-containing electrolytes is equally important in this context.

In summary, *in situ* Fe K-edge XANES reveals a spontaneous interphasial reaction between the uncharged Li_2FeSO_4 cathode and the $LiPF_6$-based electrolyte, manifested with the Fe^{2+}/Fe^{3+} ratio variation from the pristine state. Subsequent cycling of the cathode material (formation cycle) is partially restorative in Fe oxidation state.

The authors acknowledge assistance provided during data acquisition by Dr. W. Chen and Dr. C.-Y. Kim. Further acknowledgement and gratitude is extended to Dr. L. Zhang (University of Nebraska-Lincoln) for providing the reference compound data. This work is supported through a Hydro-Québec/Natural Sciences & Engineering Research Council of Canada (NSERC) Collaborative R&D research grant. DTJ acknowledges Canadian NSERC support for the work done at the University of Guelph. Synchrotron radiation measurements were performed at the CLS, which is supported by CFI, NSERC of Canada, University of Saskatchewan, Government of Saskatchewan, Western Economic Diversification Canada, NRC Canada, and CIHR.

Notes and references

‡ Heterogeneity of unique local ionic environments offers on average a higher continuity of available states. In effect, XANES peak broadening can be due to the presence of multiple crystalline phases, or, as is the case here, from increased local structure disorder within the same phase.

1. J. M. Tarascon and M. Armand, *Nature*, 2001, **414**, 359-367.
2. J. B. Goodenough and K.-S. Park, *J. Amer. Chem. Soc.*, 2013, **135**, 1167-1176.
3. M. E. Arroyo-de Dompablo, M. Armand, J. M. Tarascon and U. Amador, *Electrochem. Comm.*, 2006, **8**, 1292-1298.
4. A. Nytén, A. Abouimrane, M. Armand, T. Gustafsson and J. O. Thomas, *Electrochem. Comm.*, 2005, **7**, 156-160.
5. M. S. Islam, R. Dominko, C. Masquelier, C. Sirisopanaporn, A. R. Armstrong and P. G. Bruce, *J. Mater. Chem.*, 2011, **21**, 9811-9818.
6. D. Lv, J. Bai, P. Zhang, S. Wu, Y. Li, W. Wen, Z. Jiang, J. Mi, Z. Zhu and Y. Yang, *Chem. Mater.*, 2013, **25**, 2014-2020.
7. A. W. Brownrigg, G. Mountjoy, A. V. Chadwick, M. Alfredsson, W. Bras, J. Billaud, A. R. Armstrong, P. G. Bruce, R. Dominko and E. M. Kelder, *J. Mater.Chem. A*, 2015, DOI: 10.1039/C4TA06305H.
8. A. R. Armstrong, N. Kuganathan, M. S. Islam and P. G. Bruce, *J. Amer. Chem. Soc.*, 2011, **133**, 13031-13035.
9. J. B. Goodenough and Y. Kim, *Chem. Mater.*, 2010, **22**, 587-603.
10. Y. Li, M. Bettge, B. Polzin, Y. Zhu, M. Balasubramanian and D. P. Abraham, *J. Electrochem. Soc.*, 2013, **160**, A3006-A3019.
11. C. Dippel, S. Krueger, V. Kraft, S. Nowak, M. Winter and J. Li, *Electrochim. Acta*, 2013, **105**, 542-546.
12. D. Ensling, M. Stjerndahl, A. Nyten, T. Gustafsson and J. O. Thomas, *J. Mater. Chem.*, 2009, **19**, 82-88.
13. C. Dippel, S. Krueger, R. Kloepsch, P. Niehoff, B. Hoffmann, S. Nowak, S. Passerini, M. Winter and J. Li, *Electrochim. Acta*, 2012, **85**, 66-71.
14. K. Xu, *Chem. Rev.*, 2014, **114**, 11503-11618.
15. X. Lu, H. Wei, H.-C. Chiu, R. Gauvin, P. Hovington, A. Guerfi, K. Zaghib and G. P. Demopoulos, *Sci. Rep.*, 2015, **5**. 8599
16. C. A. Schneider, W. S. Rasband and K. W. Eliceiri, *Nat Meth*, 2012, **9**, 671-675.
17. D. T. Jiang, N. Chen and W. Sheng, *AIP Proc.*, 2007, **879**, 800-803.
18. B. Ravel and M. Newville, *J. Synchrotron Rad.*, 2005, 12, 537-541.
19. A. P. Hammersley, S. O. Svensson, M. Hanfland, A. N. Fitch and D. Hausermann, *High Press. Res.*, 1996, **14**, 235-248.
20. C. Eames, A. Armstrong, P. Bruce and M. Islam, *Chem. Mater.*, 2012, **24**, 2155-2161.
21. G. Frank de, V. György and G. Pieter, *J Phys.: Condens. Matter*, 2009, **21**, 104207.
22. T. E. Westre, P. Kennepohl, J. G. DeWitt, B. Hedman, K. O. Hodgson and E. I. Solomon, *J. Amer. Chem. Soc.*, 1997, **119**, 6297-6314.
23. L. Zhang, 2015.

